Shallow Water Conservation Laws on a Sphere

Richard Liska and Burton Wendroff

Abstract. The conservative flux-form of the shallow water equations on a sphere is transformed to non-orthogonal gnomonic coordinates on a spherical cube and numerically tackled by a 2D composite scheme. Presented numerical results include a standard test set of shallow water problems on a rotating sphere and several Riemann problems on non-rotating and rotating spheres.

1. Introduction

Recently the problem of solving the shallow water equations (SWEs) on a sphere has attracted growing interest. SWEs on a sphere in longitude-latitude coordinates have singularities at the poles causing the so called poles problem. Several approaches have been employed to avoid this problem. A classical method for solving SWEs on a sphere is the spectral transform method (STM)[1]. Swarztrauber et. al. [2] restated SWEs on a sphere in Cartesian coordinates, Taylor et. al. [3] projected the sphere on a cube before applying the spectral element method, Ronchi et.al. [4] used "cubed sphere" approach involving a gnomonic non-orthogonal coordinate system with an equiangular mesh, while Rancic et.al. [5] compare gnomonic and conformal coordinates on a spherical cube. Cubic gnomonic projection coordinates were first used by Sadourny [6]. Spotz et.al. [7] used a fast pseudospectral method with a spherical harmonic filter. Williamson et.al. [8] have standardized the tests used for SWEs on a rotating sphere. All these tests consider smooth flows and also all the methods have been developed and tested on smooth flows. We investigate the possibility of discontinuous solutions including shock waves for which we have to state the SWEs on a sphere in flux form.

2. Shallow Water Equations on a Sphere

The shallow water equations on a rotating sphere in flux form are [8]

$$h_t + \nabla \cdot (h\mathbf{v}) = 0 \tag{1}$$

$$(h\mathbf{v})_t + \nabla \cdot (\mathbf{v}h\mathbf{v}) + gh\nabla H + f\mathbf{r}_0 \times h\mathbf{v} = 0 \tag{2}$$

where h is the thickness of the fluid, H is the height of the upper surface of the fluid (i.e. $H = h + h_0$, where h_0 is the bottom profile topography), $\mathbf{v}$ is the horizontal (on the sphere) velocity of the fluid, g is gravitation constant, $\mathbf{r}_0$ is the outward unit radial vector and f is the Coriolis parameter, $f = 2\Omega \sin\Theta$ with Ω being rotation rate of the sphere and Θ the latitude. In longitude $\lambda \in (-\pi, \pi)$ and latitude $\Theta \in (-\pi/2, \pi/2)$ coordinates the velocity $\mathbf{v}$ has components u and v respectively.

2.1. 1D Rotational Symmetry Cases

First we suppose that the sphere is not rotating, i.e. $f = 0$, and assume rotational symmetry, i.e. we assume that the solution is independent of the longitude, with zero longitudinal velocity $u = 0$. Under these assumptions the shallow water equations (1), (2) can be written as

$$\begin{aligned} (h\cos\Theta)_t + \left(\frac{hv\cos\Theta}{a}\right)_\Theta &= 0 \\ (hv\cos\Theta)_t + \left(\frac{\cos\Theta}{a}(hv^2 + \frac{1}{2}gh^2)\right)_\Theta + \frac{1}{2a}gh^2\sin\Theta &= 0 \end{aligned} \tag{3}$$

where we avoided the singularities at the poles by introducing the conserved quantities $h\cos\Theta$ and $hv\cos\Theta$ (a is the radius of the sphere). Close to the poles the above system can be approximated by the planar radially symmetric case.

On the rotating sphere we have to include the Coriolis force ($f \neq 0$) and even in the rotational symmetry case when the solution does not depend on the longitude we cannot assume zero longitudinal velocity u. When we apply just the assumption that nothing depends on λ then the SWEs (1), (2) can be for flat bottom ($h_0 = 0$) written as

$$\begin{aligned} (h\cos\Theta)_t + \left(\frac{hv\cos\Theta}{a}\right)_\Theta &= 0 \\ (hu\cos\Theta)_t + \left(\frac{huv\cos\Theta}{a}\right)_\Theta - \left(f\cos\Theta + \frac{u}{a}\sin\Theta\right)hv &= 0 \\ (hv\cos\Theta)_t + \left(\frac{\cos\Theta}{a}(hv^2 + \frac{1}{2}gh^2)\right)_\Theta + \frac{1}{2a}gh^2\sin\Theta & \\ + \left(f\cos\Theta + \frac{u}{a}\sin\Theta\right)hu &= 0 \end{aligned} \tag{4}$$

where again we avoided the singularities at the poles by introducing the conserved quantities $h\cos\Theta, hu\cos\Theta$ and $hv\cos\Theta$.

2.2. Flux Form of Equations in Gnomonic Coordinates on a Spherical Cube

Gnomonic coordinates on a spherical cube have been first used by Sadourny [6], more recently this idea has been used in [4]. In [5] gnomonic coordinates are compared with conformal coordinates on a spherical cube. Here we follow the "cubed sphere" method from [4]. A spherical cube is obtained by projecting the edges of a cube on the surface of a sphere. The gnomonic coordinates define on each face of the spherical cube local coordinates as two angles $(\xi, \eta), \xi \in (-\pi/4, \pi/4), \eta \in (-\pi/4, \pi/4)$. The central point of the face has local coordinates $(0, 0)$ and the edges of the spherical cube have one of the local coordinates equal to $\pm\pi/4$. Two central points coincide with two poles and the other four are on the equator. On a face divided by the equator the local coordinate ξ is just the shifted longitude. ξ is the angle of two planes intersecting at the rotation axis going through the poles, the first plane includes the center of the face and the other one includes given point. For the local coordinate η on this face we introduce a new axis going through two centers of neighboring equatorial faces in west and east directions. η is the angle of two planes intersecting at this second axis, the first plane includes the center of our face (it includes the whole equator) and the other one includes given point. Local coordinates on the other faces are defined similarly by introducing the third symmetry axis of the sphere which is orthogonal to both previous axes. In fact gnomonic coordinates are defined by rotating around these three axes.

The shallow water equations (1),(2) expressed in the local coordinates (ξ,η) are the same in all faces. As we are interested in the shallow water equations as a system of conservation laws, in order to correctly treat discontinuous shock waves we need to derive them in a flux form,

$$\begin{aligned} h_t + (q^\xi v^\xi h)_\xi + (q^\eta v^\eta h)_\eta + p^\xi v^\xi h + p^\eta v^\eta h &= 0 \\ (v^\xi h)_t + (q^\xi {v^\xi}^2 h + r^{\xi\xi} h^2)_\xi + (q^\eta v^\xi v^\eta h + r^{\xi\eta} h^2)_\eta & \\ + p^\xi {v^\xi}^2 h + t^\xi v^\xi v^\eta h + o^\xi h^2 + s^\xi v^\xi h - s^\eta v^\eta h &= 0 \\ (v^\eta h)_t + (q^\xi v^\xi v^\eta h + r^{\eta\xi} h^2)_\xi + (q^\eta {v^\eta}^2 h + r^{\eta\eta} h^2)_\eta & \\ + p^\eta {v^\eta}^2 h + t^\eta v^\xi v^\eta h + o^\eta h^2 + s^\eta v^\xi h - s^\xi v^\eta h &= 0. \end{aligned} \tag{5}$$

The coefficients $q^\xi, q^\eta, p^\xi, p^\eta, r^{\xi\xi}, r^{\xi\eta}, r^{\eta\xi}, r^{\eta\eta}, t^\xi, t^\eta, o^\xi, o^\eta, s^\xi, s^\eta$ appearing in the equations depend on $\tan\xi, \tan\eta, a, g$.

The system (5) is a system of conservation laws for the conserved quantities $h, v^\xi h, v^\eta h$. v^ξ and v^η are the ξ and η components of the velocity vector $\mathbf{v}$ in the local coordinate system.

3. Discretization

For a system of conservation laws with sources $U_t + f_x(U) = s(U,x)$ in 1D the two-step Lax-Friedrichs (LF) scheme defines new values on a staggered dual grid as

$$\begin{aligned} U_{i+1/2}^{n+1/2} &= \frac{1}{2}[U_i^n + U_{i+1}^n] - \frac{\Delta t}{2\Delta x}[f(U_{i+1}^n) - f(U_i^n)] \\ &\quad + \frac{\Delta t}{2} s((U_{i+1}^n + U_i^n)/2, x_{i+1/2}), \end{aligned} \tag{6}$$

and the solution on the original grid is obtained by the same formula shifted by $1/2$ in the indices n, i. The sources are treated in a simple way. The two-step Lax-Wendroff (LW) scheme uses the same predictor (6) for the first half step. In the second half step it advances from the time level n to the time level $n+1$ using the fluxes from the time level $n+1/2$,

$$U_i^{n+1} = U_i^n + \frac{\Delta t}{\Delta x}[f(U_{i+1/2}^{n+1/2}) - f(U_{i-1/2}^{n+1/2})] + \Delta t s((U_{i+1/2}^{n+1/2} + U_{i-1/2}^{n+1/2})/2, x_i). \tag{7}$$

It is well known that the LW scheme produces oscillations behind shocks while LF is excessively diffusive, smearing out the shocks. However, a combination of these two schemes that we call a composite scheme has proved to work well in many cases [9]. The composite scheme is defined by global composition of several LW steps followed by one LF step. We denote by L_W the operator defined by the LW scheme (6),(7) and by L_F the operator defined by the LF scheme (6). The difference operator $S_k = L_F \circ L_W \circ \cdots \circ L_W$, defined by $k-1$ applications of L_W followed by one application of L_F then defines the composite scheme which we call LWLFk. The operator S_k operates from time level n to $n+k$, $U^{n+k} = S_k U^n$. The time step in our computations is determined by $\sigma \Delta t/\Delta x \leq CFL$, where σ is the maximum absolute value of the flux Jacobian eigenvalues. All schemes are stable up to $CFL = 1$ and we use CFL close to 1.

In 2D we also use composite schemes using our new version of the 2D LF scheme and a second order corrected Lax-Friedrichs (CF) scheme [9]. The LF half step (analogous to (6) in 1D) first approximately solves the 1D Riemann problems at the middle of cell edges at the $n+1/4$ time level and then uses the fluxes at these new values to compute values at time level $n+1/2$. The CF corrector is an analogue of 1D (7). The time step in computations is determined adaptively from the condition $\max(\sigma_x \Delta t/\Delta x, \sigma_y \Delta t/\Delta y) \leq CFL$ where σ_x and σ_y are maximum absolute values of the x and y flux Jacobian eigenvalues. Both schemes are again optimally stable up to $CFL = 1$ [9]. In the computations we use CFL close to 1.

An important issue is the treatment of the boundaries between the different regions of the sphere. We use a slight modification of the composite mesh method used in [4]. As we are using a predictor-corrector type of difference scheme it is for us sufficient to use the additional boundary conditions from the adjoining regions during the predictor step on the dual grid. As the predictor step is first order the boundary conditions need to be only first order too, so we need not take care of precision on the boundaries and use the simplest 1D (for each pair of neighboring regions one local coordinate of one region is the same as one local coordinate of the other one, except a constant shift) linear interpolation to get values at desired locations. On the grid lines $\xi = 0$ or $\eta = 0$ going through the centers of cubed sphere faces both adjacent local coordinates match exactly (one is zero) at the centers of cubed sphere edges and the boundary conditions are completely transparent around the centers of the edges. We have not observed any reflections of waves from the internal borders, however, as might be expected, waves passing over the cubed sphere corners are deformed more than waves passing over the grid lines $\xi = 0$ or $\eta = 0$. Using this approach we have not noticed any noise generated on the boundaries, such as reported in [6] or [4] (of course we use only first or second order schemes, while in [4] a fourth order scheme has been used). This remains true also for smooth problems solved by the second order scheme and we do not need to apply any filter, artificial viscosity or fourth order hyperdiffusion (in [4] the Assalin filter with hyperdiffusion has been used).

4. Numerical Results

4.1. Standard Test Set

Although we are interested in discontinuous solutions we first check how our method works for smooth flows on the standard test set for the shallow water equations on the surface of a sphere [8] for which we can compare with results of others. The results are summarized in the Table 1 showing the normalized l_2 errors for standard test cases using an $N \times N$ grid on each face, with $N = 23, 45, 90$ corresponding to grid step of $4°, 2°, 1°$, together with the results of the STM [1] and the Cartesian method on an icosahedral geodesic grid [2]. To compare the resolutions we have included also the number of grid points for each case. Our results are comparable with those of the Cartesian method for the test 1 and better for the test 3 (other tests were not presented in [2]). STM gives better results for the test 1 and comparable results to ours for the tests 4,5,6,7a. The tests 2 and 3 are trivial for STM giving negligible errors. Test cases 1-4 have an analytical solution so one can easily compute the numerical error of their results. For the other tests we compare our results with the T213 high resolution STM results available at `ftp://ftp.ucar.edu/chammp/shallow/`.

Reso-	Nr .				Test			
lution	points	1	2	3	4	5	6	7a
O23	2 904	0.85	0.0023	0.0014	0.0014	0.0068	0.011	0.0059
O45	11 616	0.46	0.0005	0.00032	0.00054	0.0028	0.0032	0.0044
O90	48 600	0.14	0.0001	0.00007	0.00013	0.0009	0.0012	0.0023
T21	2 048	0.042	10^{-13}	10^{-6}	0.39	0.019	0.014	0.0073
T42	8 192	0.011	10^{-13}	10^{-10}	0.00082	0.00096	0.0044	0.0035
T85	32 768	0.005	10^{-13}	10^{-13}	0.00040	0.00077	0.0011	0.0019
C17	5 120	1.08		0.009				
C33	10 242	0.54		0.002				
C65	40 962	0.15		0.0007				

TABLE 1. Normalized l_2 height errors for standard test cases on rotating sphere, for our method (resolutions O23, O45, O90), for STM (resolutions T21, T42, T85 - data taken from [7]) and for the Cartesian method (resolutions C17, C33, C65).

4.2. Dam Break Problem on Non-rotating Sphere

The dam break problem is defined by the initial conditions

$$\begin{aligned} h &= \begin{cases} 1000 & \Theta + \pi/2 \leq 0.3 \\ 100 & \Theta + \pi/2 > 0.3 \end{cases} \\ v &= 0 \end{aligned} \tag{8}$$

This example represents a broken circular dam at the south pole. The physical constants in all our examples are those of the earth, namely, $a = 6\ 371\ 220\ m, g = 9.806\ 16\ ms^{-2}$, the sphere is non-rotating, here $\Omega = 0$. The dam break problem does not correspond to any practical problem related to the atmosphere or the ocean on earth, however, this Riemann problem is of theoretical interest.

The results of a computation with 90×90 cells (i.e. one cell per one degree) in each of the six regions of the spherical cube using the CFLF4 scheme with $CFL = 1$ are compared with 1D results of the model (3) using 2000 points in Fig. 1. Excellent agreement has been achieved.

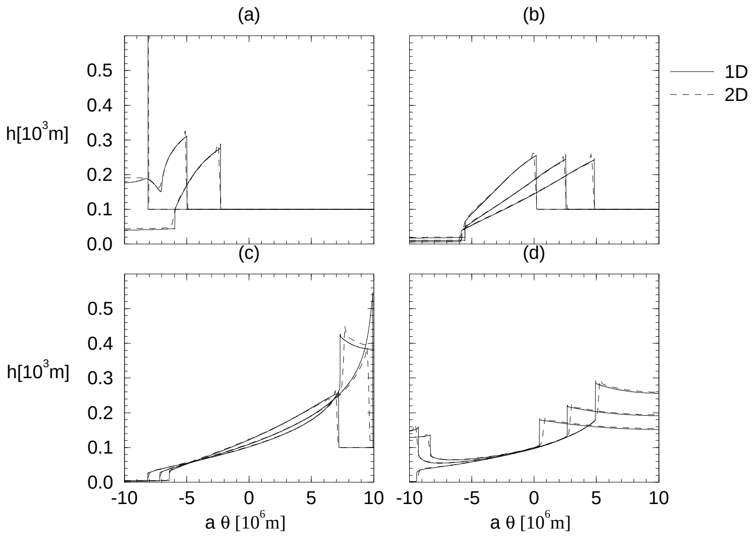

FIGURE 1. Heights comparison of 1D and 2D (on the half circle $\lambda = 0$) shallow water rotational symmetric dam break problem flow on non-rotating sphere at times (a) 0, 10, 20 hours, (b) 30, 40, 50 hours (c) 60, 70, 80 hours and (d) 90, 100, 110 hours.

The jump at the generated shock first decreases and then it increases as the shock approaches the north pole ($a\Theta = 10^7 m$) from which the shock is reflected. The second shock at the tail of the rarefaction wave first travels in the same direction as the first one, some time after the first one crosses the equator ($a\Theta = 0$)

the second shock starts to travel backwards and when it reaches the south pole ($a\Theta = -10^7 m$) it is reflected from it.

The rotational symmetry of the solution is preserved very well as might be seen in Fig. 2 where the plotted heights have been amplified by 5000 to make the surface structure distinguishable from the sphere surface. For this figure we computed with 90×90 cells in each of the regions however the grid is displayed only in 45×45 resolution so that one can distinguish the grid lines on the 3D surface. In Fig. 2(a) the circular shock around the south pole at $t = 10$ hours can be seen, Fig. 2(b) shows the shock at $t = 30$ hours located around the equator, Fig. 2(c) catches the shock at $t = 80$ hours after its reflection from the north pole and finally Fig. 2(d) presents a small circular shock reflected from the south pole and the first shock returning from the north pole which is located close to the equator (compare also with Fig. 1 presenting 1D results).

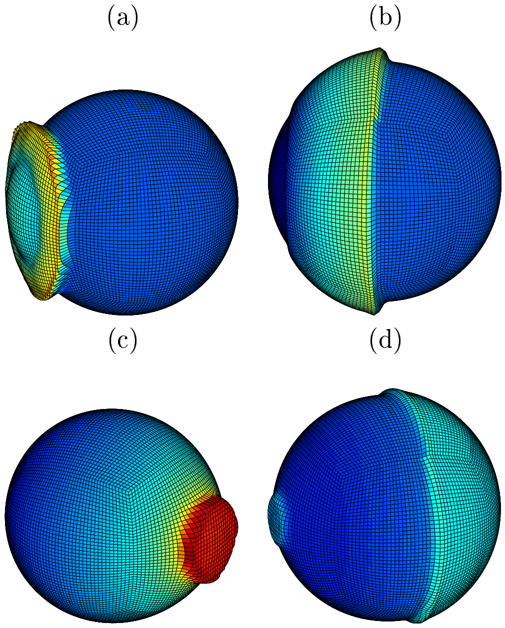

FIGURE 2. Dam break on the non-rotating sphere at times (a) 10 hours, (b) 30 hours (c) 80 hours and (d) 110 hours. Heights are multiplied by 5000. South pole is on the left.

4.3. Dam Break on Rotating Sphere

Here we treat again the problem of a circular dam break solved in the previous section on a non-rotating sphere, however now we solve this problem on the rotating sphere ($\Omega = 7.29210^{-5} s^{-1}$). The circular dam is centered on the south pole and the initial conditions are given by (8) and $u = v = 0$. As this problem keeps the longitudinal symmetry (Coriolis force does not depend on longitude) it can be treated in 1D by using the equations (4). 1D and 2D results computed by CFLF4 scheme with $CFL = 1$ are presented in Fig. 3. In 1D we used 2000 cells, and in the 2D spherical case we used resolution O90, i.e. 90×90 cells on each face of "cubed sphere".

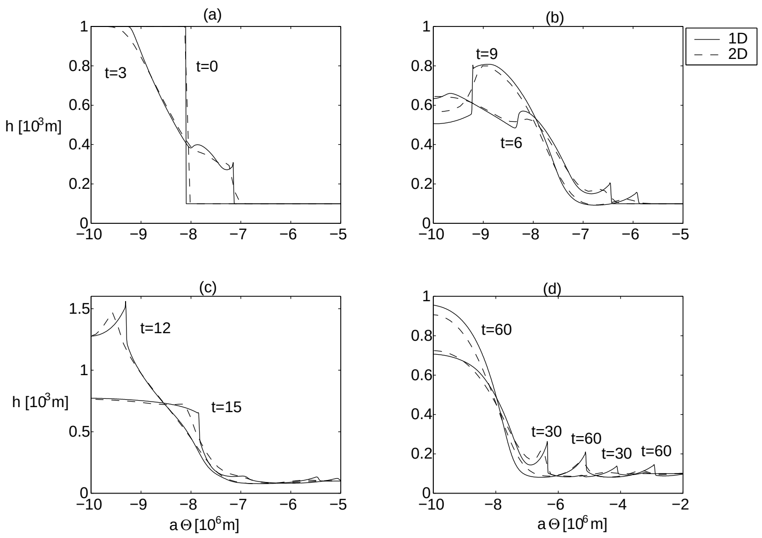

FIGURE 3. Heights comparison of 1D and 2D spherical shallow water rotational symmetric dam break problem on rotating sphere centered at the south pole at times (a) 0, 3 hours, (b) 6, 9 hours, (c) 12, 15 hours and (d) 30, 60 hours.

In Fig. 3 the south pole (the center of the dam) is located on the left at point $a\Theta = -10^7 m$ and the equator would be at point $a\Theta = 0$. At an early stage ($t = 3$) a shock wave moves right towards the equator and a rarefaction wave moves left towards the south pole and later ($t = 6, 9$) another shock wave goes left from the place of the original dam towards the south pole where it is focused between $t = 9$ and $t = 12$. The reflected shock seen at $t = 12$ gives rise to the second right going shock wave seen at $t = 30$. At later times the height of a smooth zonal flow type solution slowly oscillates around the south pole while the positions of low amplitude non-smooth waves slowly oscillate in the north-south direction. A 3D view of the water surface is shown in Fig. 4 at times $t = 9$ and $t = 30$. Clearly these results completely differ from results without rotation. As we used a much finer grid in the 1D case the results in 1D should be more precise.

(a) (b)

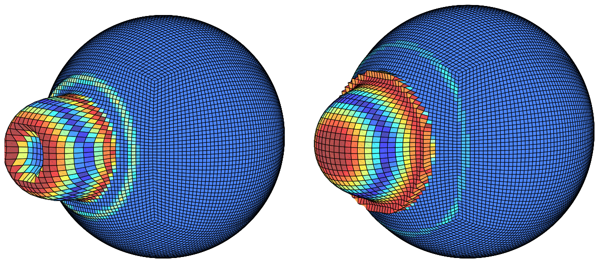

FIGURE 4. Dam break on the rotating sphere at times (a) 9 hours, (b) 30 hours computed at O90 resolution and displayed at O45 resolution. Note that the colormaps have been changed to show all waves which might be located at Fig. 3. Heights are multiplied by 5000. South pole is on the left.

Introducing rotation into our circular dam break problem shows quite a dramatic influence of the included Coriolis force source terms on the results, and of course the results depend now also on the position of the circular dam on the sphere. For the circular dam break problem at the pole the solution for large time tends to some kind of zonal flow. On the other hand, if the dam is centered on the equator the shock waves might travel on the equator where the Coriolis force is zero in both west and east directions and interfere when they meet later.

5. Conclusion

We have investigated some possibilities for the numerical treatment of discontinuous solutions of the shallow water equations (SWEs) on the surface of a non-rotating or rotating sphere. We have used composite schemes on a uniform gnomonic grid on the sphere. Their performance has been checked on the set of standard tests [8] with smooth solutions. For circular dam break problems at the pole, which can be treated by cylindrical symmetry in 1D, we have gotten excellent agreement between full 2D results on the sphere and 1D results computed on a very fine grid. The spectral transform method (STM) [2] is designed for smooth solutions and uses divergence and vorticity equations instead of momentum equations. Divergence and vorticity are important for smooth flows, however, for shocks the momentum balance is essential. The dam break problems solved by STM results in similar waves as those presented above but the shock waves are slower. The divergence and vorticity equations obtained by differentiation of the momentum equation have different weak solutions.

Acknowledgement

R. Liska was supported in part by the National Science Foundation grant CCR-9531828, by the Ministry of Education of Czech Republic program Kontakt ME 050 (1997), by the Czech Grant Agency grant 201/00/0586 and would like to thank the Institute for Geophysics and Planetary Physics (IGPP) for hosting his visit at Los Alamos National Laboratory.

References

[1] R. Jakob-Chien, J.J. Hack, and D.L. Williamson. Spectral transform solutions to shallow water test set. *J. Comp. Phys.*, 119:164–187, 1995.

[2] P.N. Swarztrauber, D.L. Williamson, and J.B. Drake. The cartesian method for solving partial differential equations in spherical geometry. *Dynamics of Atmospheres and Oceans*, 27:679–706, 1997.

[3] M. Taylor, J. Tribbia, and M. Iskandarani. The spectral element method for the shallow water equations on the sphere. *J. Comp. Phys.*, 130:92–108, 1997.

[4] C. Ronchi, R. Iacono, and P.S. Paolucci. The "cubed sphere": A new method for the solution of partial differential equations in spherical geometry. *J. Comp. Phys.*, 124:93–114, 1996.

[5] M. Rancic, R.J. Purser, and F. Mesinger. A global shallow-water model using an expanded spherical cube: Gnomonic versus conformal coordinates. *Q.J.R. Meteorol. Soc.*, 122:959–982, 1996.

[6] R. Sadourny. Conservative finite-differencing approximations of the primitive equations on quasi-uniform spherical grids. *Mon. Weather Rev.*, 100:136–144, 1972.

[7] W.F. Spotz, M.A. Taylor, and P.N. Swarztrauber. Fast shallow-water equation solvers in latitude-longitude coordinates. *J. Comp. Phys.*, 145:432–444, 1998.

[8] D.L. Williamson, J.B. Drake, J.J. Hack, R. Jakob, and P.N. Swarztrauber. A standard test set for numerical approximations to the shallow water equations in spherical geometry. *J. Comp. Phys.*, 102:211–224, 1992.

[9] R. Liska and B. Wendroff. Composite schemes for conservation laws. *SIAM J. Numer. Anal.*, 35(6):2250–2271, 1998.

Czech Technical University in Prague
Faculty of Nuclear Sciences and Physical Engineering
Břehová 7, 115 19 Prague 1, Czech Republic
E-mail address: `liska@siduri.fjfi.cvut.cz`,
`http://www-troja.fjfi.cvut.cz/~liska`

Group T-7, Los Alamos National Laboratory
Los Alamos, NM 87544, USA
E-mail address: `bbw@lanl.gov`, `http://math.unm.edu/~bbw`